Control of Oligonucleotide Distribution on the Shell of Thermo-responsive Polymer Nanoparticles

T. J. V. Prazeres, J. P. S. Farinha,* and J. M. G. Martinho

Centro de Química-Física Molecular and IN–Institute of Nanoscience and Nanotechnology, Instituto Superior Técnico, 1049-001 Lisboa, Portugal

Received: May 29, 2008; Revised Manuscript Received: June 30, 2008

We used Förster resonance energy transfer (FRET) to characterized the adsorption of single strand oligonucleotides (ODN) onto the thermo-responsive shell of polymer nanoparticles with a glassy poly(methyl methacrylate) (PMMA) core and a positively charged shell of poly(*N*-isopropyl acrylamide) (PNIPAM). The ODNs have 25 thymine units (dT_{25}) and are labeled at the 5′-terminus with either rhodamine X (dT_{25}-ROX, energy donor) or malachite green (dT_{25}-MG, energy acceptor). The kinetics of FRET was analyzed with a distribution model for energy transfer in restricted geometry, which allowed us to obtain the distribution of the ODN strands below and above the volume phase transition temperature of the PNIPAM shell (T_{VPT} ~30 °C). Below the T_{VPT} the ODN molecules adsorb to the expanded particle shell without changing the particle hydrodynamic radius. However, the distribution of ODN is not homogeneous: at low ODN concentrations, we observed preferential adsorption close to the core, while with the increase in ODN content, the distribution extends toward the shell/water interface. At these temperatures the mobility of the adsorbed ODN is very high and their environment is strongly hydrophilic. Above the T_{VPT}, the shell is collapsed onto the core, with the particle hydrodynamic radius determined by dynamic light scattering (DLS) changing from 109 nm (at 11 °C) to 72 nm (at 45 °C). The distribution of adsorbed ODNs also decreases in thickness, but to a value (14.7 ± 0.8 nm) that is larger than the shell thickness obtained by DLS (L_{shell} = 5 nm). This indicates that the ODN chains are fixed in the collapsed shell but protruding into the water phase, perpendicularly to the core. Time resolved fluorescence anisotropy results further show that the ODN rotation is strongly hindered above T_{VPT}.

Introduction

The controlled synthesis of multifunctional polymer nanoparticles has led to many new materials with promising industrial and biomedical applications.[1−7] The versatility of preparation in different sizes, shapes, and surface properties has yielded useful materials for catalysis, fluid viscosity control, bioseparation, immunoassays, biological diagnostics, sensors, therapeutic drug delivery, biomolecule carriers, etc.[4,8−12] Particularly interesting are the responsive polymer nanoparticles that react to external stimuli, such as temperature, pH, pressure, ionic strength, etc.[9,10,13−20] These particles have received much attention for their possible application in the separation of biomolecules,[4,5,13] as supports for proteins[4,7,19,21,22] and oligonucleotides,[7,8,11,19,23−26] and for drug and gene delivery.[4,12,13,19] Responsive nanoparticles have usually been prepared in the form of microgels,[13,14,27−29] which have shown some experimental problems, particularly due to low affinity for the absorption of several species. However, their performance can be improved by supporting the stimuli-responsive polymers in a more rigid, glassy, or rubbery polymer core.

Thermo-responsive core−shell nanoparticles, with a hydrophobic core and a hydrophilic thermo-responsive shell, have been prepared with glassy polystyrene (PS)[30] or poly(methyl methacrylate) (PMMA)[31] cores, and a thermo-responsive poly(N-isopropylacrylamide) (PNIPAM) shell. In water, PNIPAM exhibits a lower critical solution temperature (LCST) of ca. 31−35 °C.[32−36] At this temperature, the PNIPAM chains undergo a reversible volume phase transition from a solvated coil to a globular state. Below the volume phase transition temperature (T_{VPT}), the chain is in a coil conformation, resulting from the balance of the hydrophobic interactions between isopropyl groups and the hydrogen bonding between water and the polymer amide groups. Above T_{VPT}, the PNIPAM chains are in a globular conformation, because they are partially dehydrated, and the attractive interactions between the hydrophobic isopropyl groups predominate.[37−40]

Here, we are interested in using thermo-responsive core−shell polymer nanoparticles as a support for deoxyoligonucleotides (ODNs), for application in biological testing. To enhance the ability to adsorb the negatively charged ODN molecules, we synthesized monodisperse core−shell nanoparticles with a glassy core of PMMA and a cationic thermo-responsive shell of PNIPAM and aminoethyl methacrylate hydrochloride (AEMH), cross-linked with methylene bisacrylamide (MBA).[31]

The ODN molecules adsorbed onto the positively charged shell of the polymer nanoparticles show a strong decrease in mobility above the T_{VPT}, reflecting the collapse of the PNIPAM chains above this temperature.[26] However, nothing is known about the distribution of the ODNs in the PNIPAM shell, and the influence of the volume phase transition on this distribution. Because the adsorption of the ODNs onto the cationic shell is essentially driven by electrostatic interactions[41] and the charge density in the shell is mainly due to the initiator and the AEMH comonomer, the charge distribution should reflect the polymer density profile in the particle shell. At low temperature, when

* To whom correspondence should be addressed. E-mail: farinha@ist.utl.pt; phone: 351 218419221.

10.1021/jp804747b CCC: $40.75
Published on Web 09/30/2008

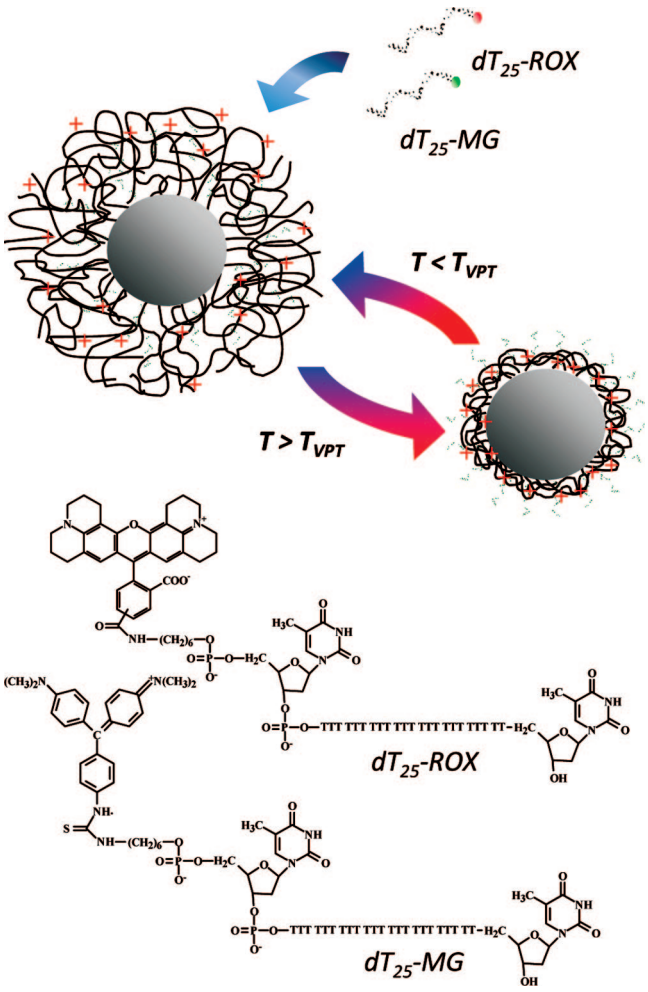

Figure 1. Förster resonance energy transfer (FRET) between polythymine oligonucleotides labeled with either rhodamine X (dT_{25}-ROX) or malachite green (dT_{25}-MG) was used to determine the distribution of the ODN molecules adsorbed onto thermo-responsive polymer core−shell nanoparticles.

the PNIPAM shell is expanded, the distribution of the adsorbed ODNs is expected to approximately reflect the particle charge distribution. However, above the T_{VPT} the PNIPAM shell collapses onto the hydrophobic core of the particle, and the ODN distribution is strongly affected.

There is not much data on the structure and conformation of polymer chains at the particle−water interface. Berndt et al.[14,29,42] have recently proposed an empirical form factor model to describe the polymer radial density profile in thermo-responsive microgels, having successfully used it to fit experimental SANS data. Here, we avoid the use of an empirical expression by modeling the structure of the thermo-responsive shell using a modification[43] of the model of Helfand and Tagami for interfaces in strongly segregated polymer systems.[44] We also use a different technique, Förster resonance energy transfer (FRET),[45,46] which allows us to determine the distribution of the adsorbed ODNs.[43,47,48] For this purpose, polythymine oligonucleotides with 25 mers (dT_{25}) labeled at the 5′-terminus with either rhodamine X (dT_{25}-ROX energy donor) or malachite green (dT_{25}-MG energy acceptor) were used (Figure 1). This donor/acceptor pair was chosen because ROX has a high quantum yield and a monoexponential fluorescence decay in aqueous solutions,[25] MG is non-fluorescent, and the critical Forster radius for this pair is high.

FRET is an important tool for characterizing different types of nanodomains[49−51] in micellar assemblies,[52−55] block copolymer micelles,[56−59] vesicles,[60−66] porous glasses,[51] Langmuir−Blodgett films,[67,68] polymer interfaces in blends,[69−72] latex particle interfaces,[43,48,73,74] biological systems,[64,66,75−78] etc. The increasing use of FRET results from the high sensitivity of this technique to the donor−acceptor distance, which can be used to obtain detailed information on their distributions on a length scale of a few nanometers.[47] Furthermore, it involves relatively simple experimental techniques, and can be successfully extended to imaging applications, in particular of biological systems.[79−82]

We have previously used FRET to characterize the core−corona interface of block copolymer micelles labeled at the block junctions with donor and acceptor dyes[57,83] and to characterize the polymer−water interface in different polymer nanoparticles.[43,48] Here, we cannot use the same methodology to characterize the particles because the dyes (such as Rhodamine X and Malachite Green) do not adsorb onto the hydrated, positively charged PNIPAM shell. However, we use a similar approach to characterize the distribution of dye-labeled ODN

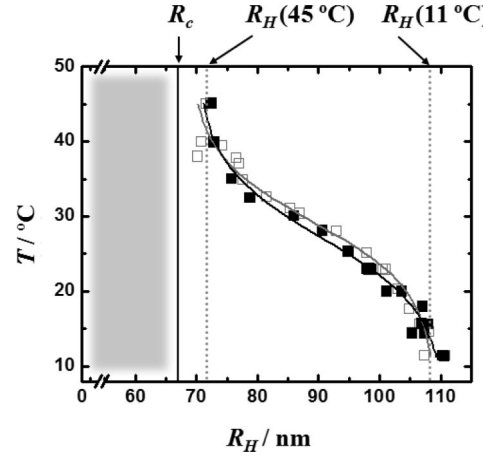

Figure 2. Hydrodynamic radii of the core (R_c) and of the particles (R_H), determined by DLS of dispersions (5.0×10^{-3} wt %) in aqueous phosphate buffer solution (1 mM, and 1 mM NaCl, pH 4) at different temperatures; (□) without ODNs adsorbed and (■) with the equivalent to the maximum adsorption of oligonucleotides used for FRET measurements. The black and gray solid lines correspond to fitting curves to the experimental data.

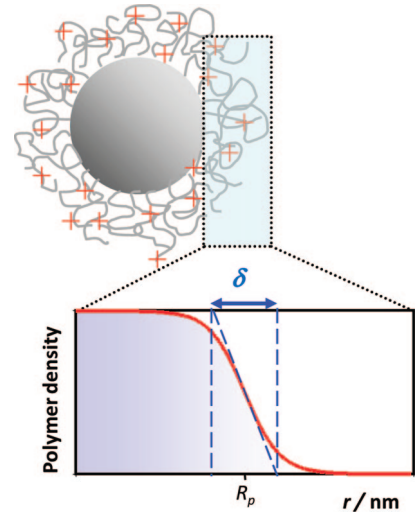

Figure 3. Schematic view of the core−shell polymer nanoparticle with average radius R_p. The density profile of positively charged groups in the particle shell is described by eq 2 (red line). The shell−water interface thickness parameter (δ) is defined from the intercepts of the tangent line at the inflection point of the density profile.

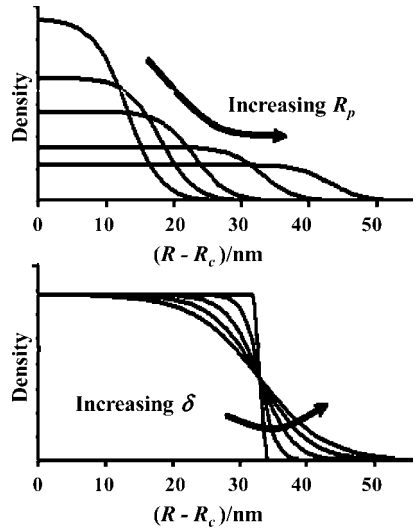

Figure 4. Simulated variation of the shell density profile with the average particle radius (top, $R_p = 80$, 85, 90, 100, and 110 nm, and constant interface thickness $\delta = 10$ nm), and with the interface thickness parameter δ (bottom, $\delta = 1$, 5, 10, 15, 20 nm, and constant particle radius $R_p = 100$ nm) for a core shell particle with core radius $R_c = 67$ nm.

molecules adsorbed onto the thermo-responsive shell of core−shell polymer nanoparticles, below and above the T_{VPT}.

Experimental Section

Materials. The dT_{25}-ROX and dT_{25}-MG oligonucleotides (Figure 1) were purchased from Thermo (Germany) in the lyophilized form (HPLC grade).

Core−Shell Nanoparticles. The polymer core−shell particles were obtained by a two-stage emulsion polymerization technique in water,[31] using methylmethacrylate (MMA, from Aldrich, 99%), N-isopropylacrylamide (NIP AM, from Acros, 99%), and aminoethylmethacrylate hydrochloride (AEMH, from Acros, 99%) monomers. 2,2′-Azobis(2-amidinopropane) dihydrochloride (V50, from Wako chemicals) was used as initiator, and dodecylethyldimethyl ammonium bromide (DEDAB, from Fluka AG, >98%) was used as surfactant. A small amount of methylene bisacrylamide (MBA, from Kodak, eletrophoretic grade) was used to cross-link the polymer chains. In the first stage, the PMMA core was prepared using a mixture of DEDAB (0.06 g/100 g of mixture, ~2 mM) at a concentration below its critical micelle concentration (CMC ≈ 13−14 mM),[84,85] V50 (0.05 g), and MMA (5 g) under N_2(g) atmosphere at a constant temperature of 70 °C, until ca. 80% conversion was reached. In the second stage, a mixture of NIPAM/MBA/AEMH (0.88 g/0.10 g/0.031 g) was added in several shots to the reaction medium at 70 °C for at least 2 h. The global conversion was 100%, and the solid content of the final particle dispersions was ca. 9.5 wt %.

The hydrodynamic radius of the particle core, $R_c = 67$ nm, was obtained by dynamic light scattering (DLS) of PMMA nanoparticles synthesized in similar conditions as those used to prepare the core of the core−shell particles.[31] The hydrodynamic radius of the core−shell particles reversibly changes from 109 nm below the T_{VPT} (11.5 °C) to a minimum of 72 nm above the T_{VPT} (45 °C). The monodispersity of both the core and the core−shell particles is attested by the low standard deviation (SD = 0.01) of the hydrodynamic radius obtained by DLS.

Sample Preparation. The ODN were dissolved in a 1 mM phosphate buffer solution (1 mM NaCl, pH 4.0), prepared using sodium dihydrogenphosphate 1-hydrate ($NaH_2PO_4 \cdot H_2O$, Panreac), hydrochloric acid (HCl, 1N, Panreac), 1 mM of sodium chloride (NaCl, Merck), and Milli-Q water. Before the measurements, the samples containing nanoparticles and ODNs were incubated at room temperature (23 °C) for at least 3 h in order to guarantee the adsorption equilibrium. For DLS and fluorescence measurements we used less than 0.0150 wt % of nanoparticles to avoid multiple scattering and contamination of the fluorescence emission by the scattered light. The maximum concentration of oligonucleotide was adjusted in order to satisfy the condition that more than 95% of the ODNs are adsorbed. This level of adsorption was confirmed by fluorescence measurements of the supernatant obtained by centrifugation of an equilibrated dispersion at 14 000 rpm for 20 min. For FRET measurements, the concentration of nanoparticles was kept constant at 0.0150 wt %, with the donor (dT_{25}-ROX) concentration at 3.6 nmol/L, whereas the concentration of acceptor (dT_{25}-MG) was changed from 5.4 to 45.3 nmol/L.

Fluorescence Spectra and Decay Curves. The absorption spectra were measured in a Shimadzu UV-3101PC spectrometer and the fluorescence spectra in a SLM-AMINCO 8100 Series 2 spectrofluorimeter, in both cases using 5 × 5 mm quartz cuvettes. For the determination of R_0 we used a bandwidth of 2 nm for emission and excitation. The spectra were corrected for the response of the detection system, and the temperature was kept at 23 °C by a water circulating bath (±0.5 °C, Julabo F25). Time-resolved fluorescence decays with picosecond resolution were obtained by the single-photon timing technique using laser excitation at 575 nm. The system consists of a mode-locked Coherent Inova 440−10 argon ion laser synchronously pumping a cavity-dumped Coherent 701−2 dye laser using Rhodamine 6G, which delivers 5−6 ps pulses at a repetition rate of 800 kHz. The fluorescence emission was observed at 615 nm using a cutoff filter to effectively eliminate the scattered light from the sample. The fluorescence was selected by a Jobin−Yvon HR320 monochromator with a grating of 100 lines/mm and detected by a Hamamatsu 2809U-01 microchannel plate photomultiplier. The experimental decay curves were fitted to simulated curves[72,86,87] using a nonlinear least-squares reconvolution method based on the Marquard algorithm.[88,89]

Dynamic Light Scattering (DLS). The hydrodynamic particle radii were obtained by dynamic light scattering (Brookhaven Instruments: BI-200SM goniometer and BI-9000AT autocorrelator) using a He−Ne laser (Spectra Physics, model 127 with 35 mW at 632.8 nm) and an avalanche photodiode detector. Diluted particle dispersions (0.005 wt % of nanoparticles in 1 mM phosphate buffer solution, 1 mM NaCl, pH ~ 4) were measured at 90° under controlled temperature (±0.1 °C). The autocorrelation functions were analyzed by Laplace inversion (CONTIN).

Results and Discussion

Dynamic Light Scattering. The hydrodynamic radius of the glassy PMMA core, $R_c = 67$ nm, was measured by DLS of model PMMA nanoparticles synthesized in similar conditions as those used to prepare the core of the core−shell particles[31] and does not change in the interval of temperatures used. On the other hand, the core−shell particles change their diameter in response to changes in temperature, while maintaining a narrow size distribution (SD < 0.01 over the full temperature range). The hydrodynamic radius of the core−shell particles show a large and broad volume phase transition, centered at a temperature $T_{VPT} \approx 30$ °C (Figure 2), close to the lower critical solution temperature (LCST) of PNIPAM in water.[9,32,33,35] The

shell of the particles is positively charged at low pH (pH 4 was used throughout this work), with the charges coming from the amidine groups of the initiator (V-50) and the amino groups of the AEMH comonomer.[25,31]

At about 11 °C (far below the T_{VPT}), the particles have the highest hydrodynamic radius ($R_H \approx 109$ nm) because the PNIPAM chains of the particle shell adopt extended conformations due to hydrogen bonding with the water molecules. In fact, the equivalent polarity of the shell, determined from the solvatochromic shifts of dT_{25}-ROX, is practically identical to that of water at temperatures below T_{VPT}.[25] Because the hydrodynamic radius of the core is $R_c = 67$ nm, the length of the PNIPAM shell can be estimated as $L_{shell} = R_H - R_c = 42$ nm. At 45 °C (ca. 15 °C above the T_{VPT}) the hydrodynamic radius of the particles is reduced to $R_H \approx 72$ nm as a result of the collapse of the PNIPAM chains onto the PMMA core, induced by the dehydration of the shell.[25,90] Even though the PNIPAM shell is reduced to a thickness of only $L_{shell} = 5$ nm, corresponding to ca. 7% of its low temperature volume, previous results indicate that dT_{25}-ROX molecules adsorbed to the shell sense a quite hydrophilic environment, with an equivalent polarity equal to a mixture of 30% (v/v) of water in dioxane.[25]

In Figure 2 it is also apparent that the behavior of the particles depends only slightly on the amount of adsorbed oligonucleotides (ODNs). This indicates that this amount of adsorbed ODN is not enough to significantly change the net charge of the particles. Although the value measured before for the particle charge density ($\sigma = 9$ μmol/g)[31] would correspond to ca. 90% neutralization of the positive charges in the particle shell (for the higher amount of ODNs adsorbed), this value measures only the more accessible surface charges. In fact, the total particle charge should be equal to the charges expected from the comonomer (ca. 30 μmol/g) plus the charges resulting from the initiator (estimated as ca. 60 μmol/g). Therefore, for a total charge close to 10^2 μmol/g, the effective neutralization achieved by the adsorption of oligonucleotides is relatively small.

Oligonucleotide (ODN) Adsorption. The adsorption isotherm of dT_{25}-ROX onto core−shell particles prepared in a similar fashion as described above (but with a lower quantity of AEMH comonomer, 0.014 g) was measured before.[25] The adsorption of dT_{25}-ROX onto the particles at 22 and 40 °C (in 10 mM phosphate buffer, pH 5.5, and 10 mM NaCl) was found to follow a Hill binding isotherm. A negative cooperative effect was observed at both temperatures, being more pronounced at higher temperature. The anticooperative adsorption is probably due to the increase in electrostatic repulsion between the negatively charged ODNs and to packing constrains. This effect is stronger for temperatures above the T_{VPT}, for which the shell is collapsed and the ODN are packed closer together. The maximum amount of adsorbed ODN per gram of particles was found to be higher at 40 °C (504 nmol g^{-1}) than at 22 °C (125 nmol g^{-1}).[25]

However, this amount of adsorbed ODN results in a very low energy transfer efficiency due to the low amount of dT_{25}-MG. Because the particle concentration cannot be increased due to the scattering of the fluorescence emission,[25,26] we prepared similar particles with a higher number of positive charges in the shell (using a 2-fold increase in AEMH, to 0.031 g). With the new particles it was possible to increase the maximum amount of adsorbed ODN to 370 ODN/particle (for an adsorption higher than 95% in 1 mM phosphate buffer, 1 mM NaCl, and pH ∼ 4, as determined by fluorescence measurements of the supernatant after centrifugation of the particles). The estimated average number of oligonucleotides per particle was calculated from the ratio of ODN (3.6×10^{-9} to 4.9×10^{-8} M) and particle concentrations (∼1.35×10^{-10} M), with the molar concentration of particles being estimated from their solids content (∼0.150 g/L) and assuming that the density of the particles at 45 °C (when the PNIPAM shell is collapsed) is identical to that of bulk PMMA (1.19 g/cm^3).[91]

For the amount of ODN and particles used in the fluorescence experiments, we can assume 100% ODN adsorption and obtain reasonable fluorescence intensities for the FRET measurements without the interference of scattered light.

Distribution of the Adsorbed ODN on the PNIPAM Shell. The charge density in the particle shell is mainly due to the protonated amine groups of the charged comonomer (AEMH) and to the contribution from the positively charged terminal amidine groups of the PNIPAM chains, coming from the initiator. For a random copolymerization of AEMH and NIPAM, we expect a fairly homogeneous charge distribution throughout the particle shell; therefore, the polymer density profile should reflect the charge distribution. Because the adsorption of the ODNs essentially results from electrostatic interactions,[11,24,41] at low ODN concentration and for the noncollapsed PNIPAM shell, the distribution of the adsorbed ODN should reflect the polymer density profile.

Berndt and Richtering[14,29,42] recently proposed an empirical model that describes the radial density profile of water-dispersed thermo-responsive polymer nanoparticles with average radius R and polymer−water interface thickness σ.

$$C(r) = \begin{cases} 1, & r \le (R-\sigma) \\ 1 - \dfrac{1}{2}\dfrac{[(r-R)+\sigma]^2}{\sigma^2}, & (R-\sigma) < r \le R \\ \dfrac{1}{2}\dfrac{[(R-r)+\sigma]^2}{\sigma^2}, & R < r \le (R+\sigma) \\ 0, & r > (R+\sigma) \end{cases} \quad (1)$$

A similar distribution function can be derived from the model of Helfand and Tagami[44] for polymer interfaces in strongly segregated systems with planar symmetry. This model has previously been modified for spherical geometry and used to model the surface of polymer nanoparticles and the core−corona interface of block copolymer micelles.[43,57,70,71] Here we use a similar approach to describe the positive charge distribution in the thermo-responsive shell of the nanoparticles with core radius R_c and a total average radius R_p (Figure 3):

$$C(r) = \begin{cases} \dfrac{1}{2V_0}\{1 - \tanh[2(r-R_p)/\delta]\}, & r > R_c \\ 0, & r < R_c \end{cases} \quad (2)$$

where V_0 is a normalization factor, and δ is an interface thickness parameter that controls the shape of the distribution at R_p and is defined from the intercepts of the tangent line at the inflection point of the distribution profile.[71]

The shell density profile defined by eq 2 expands as the value of R_p increases for a constant value of the interface thickness δ, (Figure 4 top). On the other hand, for a fixed value of R_p, the interface becomes sharper as the thickness parameter δ decreases (Figure 4, bottom). The results simulated with this model were also well-described by the empirical eq 1, when the later is modified to take into account the glassy core of the particles.

The thermo-responsive shell of the particles can be approximately described by the average shell length $L = R_p - R_c$. However, this length might be misleading if the distribution is not sharp (the case of large values of δ in eq 2). To have a

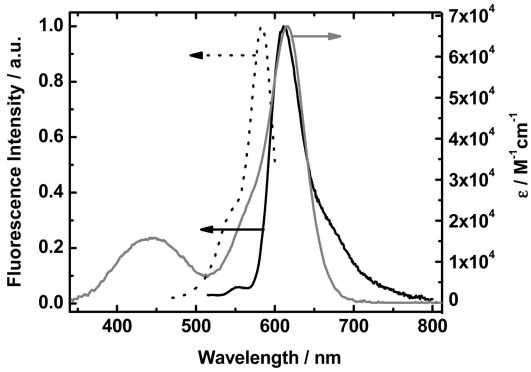

Figure 5. Normalized excitation (•••) and emission (dark line) fluorescence spectra of 9.8×10^{-7} M dT_{25}-ROX at $\lambda_{em} = 615$ nm and $\lambda_{exc} = 510$ nm, respectively, and absorption spectrum of 1.3×10^{-5} M dT_{25}-MG (light line), at 23 °C.

better estimate of the shell thickness, one should include the effect of δ. By considering $L + 0.5\delta$, only about 60% of the interface volume (defined as the integral of eq 2)[43,57,71] is considered. To include 90 and 95% of all the interface, we have to consider $L + 1.25\delta$ and $L + 1.5\delta$, respectively.

Förster Radius. The rate of FRET between an electronically excited donor molecule and an acceptor molecule separated by distance r is[45,46]

$$w(r) = \frac{3R_0^6\kappa^2}{2\tau_D}\frac{1}{r^6} \tag{3}$$

where τ_D is the unquenched donor lifetime, κ^2 is a dimensionless parameter associated with the relative orientation of the donor and acceptor transition dipole moments (dynamic averaging for a random distribution of dipoles yields $<\kappa>^2 = 2/3$),[49,92] and the Förster radius R_0 is the characteristic distance at which the rate of energy transfer is equal to the rate of intramolecular deactivation.[45,46,49,50] The value of R_0 (Å) can be calculated from eq 4,

$$R_0 = 0.2108\left(\frac{\kappa^2 Q_D}{n^4}J(\lambda)\right)^{1/6} \tag{4}$$

where Q_D is the quantum yield of the donor fluorescence in the absence of the acceptor, n is the refractive index of the medium, and N_A is Avogadro's number. The spectral overlap integral $J(\lambda)$ (in M^{-1} cm^{-1} nm^4) was determined as

$$J(\lambda) = \int_0^\infty F_D(\lambda)\varepsilon_A(\lambda)\lambda^4\, d\lambda \tag{5}$$

where $F_D(\lambda)$ is the fluorescence intensity of the donor (with the area of the spectrum normalized to 1) and $\varepsilon_A(\lambda)$ is the molar absorption coefficient of the acceptor at wavelength λ (nm).

We determined the spectral overlap integral $J(\lambda)$ from the absorption spectrum of dT_{25}-MG and the normalized emission spectra of dT_{25}-ROX (in 1.0 mM phosphate buffer, 1 mM NaCl, pH = 4) (Figure 5). The fluorescence quantum yield of dT_{25}-ROX in phosphate buffer is $Q_D = 0.9$,[25] and the fluorescence lifetime is $\tau_D = 4.7$ ns at 23 °C. The refractive index in phosphate buffer was assumed to be equal to water: $n = 1.333$. Using eq 4, we obtained $R_0 = 6.8$ nm for dynamic, randomly oriented dipoles. This value was used for the dye-labeled ODN adsorbed onto the thermo-responsive particles, since no significant change in the donor fluorescence spectrum and quantum yield, and the absorption spectra of the acceptor was detected when the particle shell collapses above the volume phase transition.

Resonance Electronic Energy Transfer in Thermo-responsive Particles. To model the FRET occurring between dT_{25}-ROX- and dT_{25}-MG-labeled ODNs adsorbed onto the thermo-responsive polymer nanoparticles at different temperatures, we associate the distribution function eq 2 with a model that accounts for the kinetics of FRET between molecules in systems with restricted geometry.[47,57,69,93,94] According to the distribution model for energy transfer in confined spherical systems,[57,69] the decay of the fluorescence emission $I_D(t)$ of the donor in the presence of acceptors is

$$I_D(t) = \exp\left(-\frac{t}{\tau_D}\right)\int_{V_s} C_D(r_D)\phi(t, r_D)r_D^2\, dr_D \tag{6a}$$

$$\phi(t, r_D) = \exp\left(-\frac{2\pi}{r_D}\int_{R_e}^\infty \{1 - \exp[-w(r)t]\}[\int_{|r_D-r|}^{r_D+r} C_A(r_A)r_A\, dr_A]r\, dr\right) \tag{6b}$$

where V_s is the volume containing all donors in the particle, and $C_D(r)$ and $C_A(r)$ are the concentration profiles of donors and acceptors, respectively. The fluorescence experimental decay, $I_D(t)$, can be determined only up to a constant factor, so the donor concentration profile is given by $C_D(r) = C(r)$, with $C(r)$ defined in eq 2. The acceptor concentration profile $C_A(r)$ has units of number density and is given by $C_A(r) = n_A C(r)$, where n_A is the total number of acceptor molecules adsorbed on each particle. The encounter radius, R_e, is the minimum distance between donor and acceptor (usually set equal to the sum of the donor and acceptor van der Waals radii).[43,57,69]

In this model we do not consider the effect of a non-homogeneous distribution of the dyes among different polymer particles. In fact, since the number of dyes per particle obeys a Poisson distribution with mean equal to the average number of dyes per particle, eq 6a should be calculated for all the different numbers of acceptor dyes per particle given by the Poisson distribution, and then the resulting decay curves are weighted with the same distribution. We have simulated these decay curves and have compared them with the donor decay curves obtained by considering only the average number of dyes in eq 6. For the dye concentration used in this work, the maximum difference between the curves was 0.01%, thus we use the average number of dyes per particle in the analysis of the experimental donor decay curves.

Distribution of the ODN Adsorbed on the Nanoparticles. The donor fluorescence decay curves of nanoparticle dispersions containing different ratios of adsorbed dT_{25}-ROX and dT_{25}-MG were fitted with eq 6, to obtain the distribution of adsorbed ODN in the particle shell (eq 2) for temperatures below and above the T_{VPT}. There are only three fitting parameters in the model: the average distribution radius R_p, the shell-water interface thickness δ, and a normalization factor for the intensity of the decay curve. The number of acceptor molecules in the shell was independently calculated from the mass balance of adsorbed dT_{25}-MG. The critical Förster distance was kept fixed to the experimental value $R_0 = 6.8$ nm, the encounter radius was set at $R_e = 0.5$ nm,[57] and the dipole−dipole relative orientation parameter was set at $<\kappa^2> = 2/3$, corresponding to rapidly rotating randomly oriented dipoles. The donor lifetime was also independently obtained from a dispersion containing only dT_{25}-ROX adsorbed to the particles, for which the fluorescence decay curves obtained at 23 and 45 °C could be fitted to a single-exponential function with lifetimes $\tau_D = 4.7$ ns and $\tau_D = 4.6$ ns, respectively. This small difference was observed before[25] and can be explained in terms of the increase in refractive index

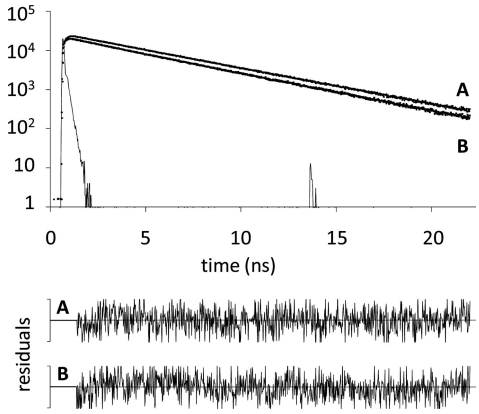

Figure 6. Time-resolved fluorescence decay curves (λ_{exc} = 575 nm, λ_{em} = 615 nm) of dT_{25}-ROX (3.6 nmol/L) adsorbed in a 0.015 wt % dispersion of polymer nanoparticles (1 mM phosphate buffer solution with 1 mM NaCl and pH 4.0) at 23 °C with 5.4 nmol/L (40 molecules/particle, **A**) and 45.3 nmol/L (340 molecules/particle, **B**) of dT_{25}-MG. The weighted residuals obtained from fitting the decay with eqs 2 and 6 are randomly distributed in both cases.

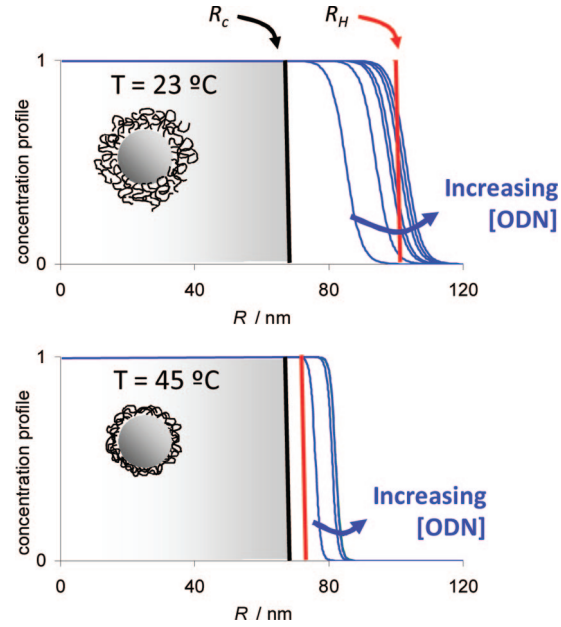

Figure 7. Distribution profiles of ODN adsorbed onto the core−shell particles at 23 and 45 °C, calculated by fitting the donor fluorescence decay curves with eqs 2 and 6 (density functions are plotted normalized to one in the maximum). As the amount of adsorbed ODN increases, the distribution of ODN becomes broader (solid blue curves). Also shown, is the hydrodynamic radii of the core R_c (dark line defining the gray region) and the hydrodynamic radii of the particles R_H (red line).

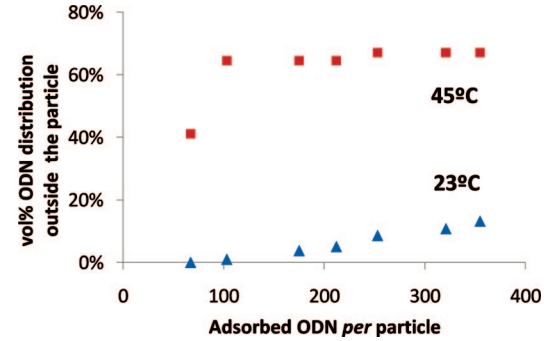

Figure 8. The volume of the ODN distribution outside the particle volume determined by DLS is much larger at 45 °C (■) than at 23 °C (▲). While at 23 °C, almost all the adsorbed ODN are located inside the PNIPAM shell; at 45 °C the shell is collapsed and the ODNs extend into the water phase.

due to the more compact structure of the PNIPAM shell above the volume phase transition temperature.

In Figure 6 we show the fluorescence decay curves (λ_{exc} = 575 nm, λ_{em} = 615 nm) measured at 23 °C for dT_{25}-ROX (3.6 nmol/L) in a 0.015 wt % dispersion of polymer nanoparticles (1 mM phosphate buffer solution, 1 mM NaCl, pH = 4.0) with 5.4 nmol/L and 45.3 nmol/L of dT_{25}-MG. Both dispersions contained an average of 27 adsorbed donor molecules per particle but different amounts of acceptor (40 and 340 acceptor molecules per particle). The decay curves were well-fitted with eqs 2 and 6, yielding randomly distributed weighted residuals and autocorrelation of the residuals. We repeated this fitting procedure for different donor/acceptor ratios while maintaining constant the number of donor molecules per particle.

From eq 2 we obtain the distribution of ODN adsorbed on the PNIPAM shell for each acceptor labeled ODN concentration (Figure 7).

The main characteristic of Figure 7 is that the ODN are distributed over a larger volume for temperatures below the volume phase transition ($T_{VPT} \approx 30$ °C). This was expected from the particle hydrodynamic radius determined by DLS. The fact that the recovered distributions are quite broad means that some of the ODN molecules should have the dye-labeled end closer to the core and others have it closer to the water phase.

We also observe that the ODN distribution changes when the amount of adsorbed ODN is changed. With the increase in adsorbed ODNs, their distribution becomes broader, with the effect being more pronounced at 23 °C, when the PNIPAM shell is expanded. However, the most unexpected feature of the results is that at 45 °C the ODN distribution stretches out of the particle hydrodynamic radius. This had not been detected by DLS probably because the low amount of ODN molecules per particle is not enough to change the hydrodynamic radius of the particle, as observed in Figure 2.

The amount of ODN that are in the water phase can be estimated from the integral of the ODN distribution that lays outside the particle hydrodynamic volume determined by DLS. While at 23 °C, the adsorbed ODN are located inside the PNIPAM shell; at 45 °C, the volume fraction of ODN outside the particle shell is larger than 60%, for more than 100 ODN/particle (Figure 8).

Figure 7 also indicates that the ODN are not homogeneously distributed across the PNIPAM shell. This effect is more clear when we plot the average length of the adsorbed ODN distribution R_p (from eq 2) and the hydrodynamic radius of the particle R_H determined by DLS, as a function of the number of adsorbed ODN per particle (Figure 9). At 23 °C, although the PNIPAM shell is swelled with water to an average length $L \approx R_p - R_c = 33$ nm (the water content at this temperature is estimated to be above 90%),[26] the ODN molecules are preferentially adsorbed near the PMMA core, gradually occupying the remainder of the shell as the ODN content is increased. For the higher amounts of ODN adsorbed, the breadth of the distribution obtained by FRET coincides with the hydrodynamic radius of the particles obtained by DLS, assuring us that the two techniques yield equivalent results. The size of the particles is not affected by the adsorption of ODN molecules in the concentrations used here (cf. Figure 2), probably because the number of negative charges coming from the ODNs (25 per molecule, resulting in a maximum of ca. 10^4 per particle) is small compared to the amount of positive charges resulting from

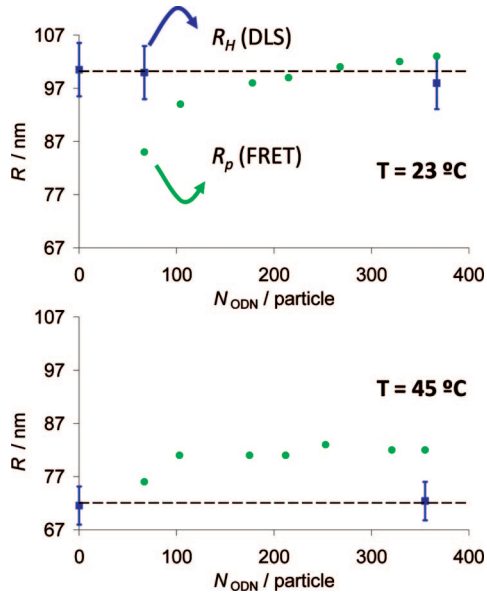

Figure 9. ODN distribution radius determined by FRET R_p, as a function of ODN molecules adsorbed per particle (●), compared to the particle hydrodynamic radius R_H determined by DLS (■, average particle hydrodynamic radius represented by the dashed line). The particle core radius is $R_c = 67$ nm.

the charged comonomer plus the initiator residues in each particle (ca. 10^5 per particle).

When the temperature is increased to 45 °C, the PNIPAM shell collapses to about 10% of its volume at 23 °C. Although the shell is only ca. 5 nm thick, it is able to keep all the adsorbed ODN, with no ODN release to the water phase being observed. The most striking feature of the ODN distributions at 45 °C is that they are considerably broader than the PNIPAM shell for all the ODN concentrations tested, especially for more than 100 ODN/particle. This means that the ODN molecules remain adsorbed to the collapsed PNIPAM shell at one end, while the rest of the molecule extends into the water.

The length of the ODN strand is estimated as ca. 8 nm (both by MD simulations and from the statistical monomer length).[95] By comparing this value with the distribution length of ca. (14.7 ± 0.8) nm, obtained at 45 °C for more than 100 ODN/particle, and the corresponding average shell thickness $L_{shell} = 5$ nm, we conclude that the ODN molecules should be relatively aligned perpendicularly to the particle surface, stretching into the water phase.

The results obtained by FRET correlate well with data obtained by fluorescence anisotropy for dT_{25}-ROX adsorbed into identical core−shell particles. The fluorescence anisotropy decays yield two rotation correlation times: the shorter correlation time corresponds to the rotation of the fluorescence probe at the tip of the ODN, θ_{ROX}, whereas the larger is related to the rotation of ODN molecule as a whole, θ_{ODN}.[25] Below the T_{VPT}, the adsorbed ODNs show rotation relaxation times identical to the ones obtained for the free ODN in water, confirming the very open structure of the PNIPAM shell with high water content. Above the T_{VPT}, the anchoring of the adsorbed ODN to the collapsed particle shell results in a more rigid conformation, which is also detected by fluorescence anisotropy measurements. At 45 °C the larger relaxation time, θ_{ODN}, is much lower when the ODN is adsorbed to the particles than in water. Moreover, the wobbling motion of the ODN is limited to a cone with semiangle of 28° (whereas at 23 °C the movement corresponds to a cone with semiangle of 40°).[26] From these

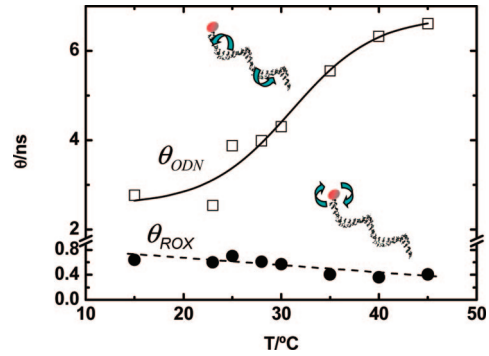

Figure 10. Rotation correlation times recovered from the analysis of the fluorescence anisotropy decays of dT_{25}-ROX adsorbed into PMMA−PNIPAM core−shell particles. The faster rotation correlation time θ_{ROX} (●) corresponds to the local motion of the dye at the end of the ODN. The longer time θ_{ODN} (□) is related to the motion of the whole ODN, which becomes more constrained above the T_{VPT}, when the ODN is anchored to the collapsed PNIPAM shell.

results we learn the maximum displacement of the probe (located at a tip of the ODN) is 0.3−0.4 nm, and thus the probes can be considered to occupy a fixed position in the time scale of energy transfer.

On the other hand, the smaller rotation correlation time θ_{ROX}, corresponding to the faster dynamics of the dye at the tip of the dT_{25}-ROX, does not show any transition at the T_{VPT} because it corresponds to a local motion, undisturbed by the PNIPAM chains of the shell (Figure 10). The fast rotation of the dye (in a time scale under 0.5 ns) justifies the assumption of rapidly rotating randomly oriented dipoles ($k^2 = 2/3$) in the energy transfer analysis.

Finally, a closer observation of Figure 7 also shows that the shape of the ODN distribution appears to be similar when the PNIPAM shell is extended (at 23 °C) and when it is collapsed with the ODN molecules protruding into the water phase (at 45 °C). In fact, the values of the δ parameter (which controls the shape of the distribution at R_p, in eq 2), obtained for the minimum global reduced χ^2 value resulting from fitting the experimental donor fluorescence decay curves for different concentrations of ODN adsorbed to the core−shell particles, only change from $\delta = 11$ nm to $\delta = 10$ nm when the temperature is increased from 23 to 45 °C. In spite of the difference in the conformation of the PNIPAM chains, the ODN molecules are mostly in an aqueous environment in both cases: while below the VPT, the ODN are adsorbed in the extended and hydrated PNIPAM shell; above the VPT, the ODN molecules are anchored to the less-polar, thin, collapsed shell of PNIPAM, but mostly extending into the water phase. We also note that at 45 °C part of the ODN molecules should be oriented with the dye toward the water phase, but the other parts probably have the dye label extremity anchored to the collapsed PNIPAM shell. The measured polarity at this temperature probably weights the two populations.[25]

Conclusions

Polymer nanoparticles with a glassy PMMA core of radius 67 nm and a positively charged thermo-responsive PNIPAM shell where used as support to adsorb single-strand ODN with 25 thymine units, labeled with either ROX (FRET donor) or MG (FRET acceptor) at the 5′-termini. The particle shell is collapsed onto the core at temperatures above the volume phase transition $T_{VPT} \approx 30$ °C but expanded below this temperature, with the particle hydrodynamic radius changing from 72 (at 45 °C) to 109 nm (at 11 °C).

The distribution of the ODNs onto the positively charged PNIPAM shell, below and above the T_{VPT}, was obtained by analyzing the kinetics of FRET with a model for energy transfer in restricted domains. Below T_{VPT} the PNIPAM shell is expanded and completely hydrated, and the radial density distributions of the adsorbed ODN molecules becomes broader as its concentration is increased, indicating that the ODN strands adsorb preferentially near the more hydrophobic particle core. The increase in ODN concentration in the shell does not result in a significant change of the particles size as shown by the DLS results. The distributions recovered are quite broad, indicating that the labeled ends of the adsorbed ODNs are distributed in the shell with the 5′-end directed either to the PMMA core or to the water phase.

When the dispersion of particles containing adsorbed ODN molecules is heated above the T_{VPT}, the ODN distribution obtained by FRET is unexpectedly much broader than the PNIPAM shell. At 40 °C, the thickness of the ODN distribution (14.7 ± 0.8 nm) is significantly larger than the shell ($L_{shell} = 5$ nm), indicating that the ODN molecules should be almost perpendicular to the particle surface and protruding into the water. This is confirmed by fluorescence anisotropy results that show that the collapse of the shell above T_{VPT} strongly hinders ODN rotation.

This way, we are able to anchor the ODN chain ends to the collapsed PNIPAM shell in a way that they do not bend due to their rigid structure while having the remaining part of the molecule in water, oriented perpendicularly to the surface. These experiments open up interesting possibilities for the use of core−shell thermo-responsive particles as supports for ODN hybridization in diagnostic tests.

Acknowledgment. The authors thank Dr A. Fedorov (CQFM) for the time-resolved fluorescence measurements and FCT (projects POCTI/47885/QUI, POCI/QUI/61045/2004, and PDCT/CTM/68451/2006) for financial support. T. J. V. P. also thanks FCT for a postdoc grant (SFRH/BPD/27175/2006).

References and Notes

(1) Smart Colloidal Materials, in *Progress in Colloid and Polymer Science*; Richtering, W. Ed.; Springer: Berlin, 2006; *Vol. 133*.

(2) Aqueous Polymer Dispersions. In *Progress in Colloid and Polymer Science*; Tauer, K. Ed.; Springer: Berlin, 2004; *Vol. 124*.

(3) *Polymer Dispersions and Their Industrial Applications*, Urban, D., Takamura, K. Eds.; Wiley-VCH: Weinheim, 2002.

(4) Kawaguchi, H. *Prog. Polym. Sci.* **2000**, *25*, 1171–1210.

(5) Kawaguchi, H.; Fujimoto, K. *Bioseparation* **1998**, *7*, 253–258.

(6) Pichot, C. *Polym. Adv. Technol.* **1995**, *6*, 427–434.

(7) Pichot, C. *Curr. Opin. Colloid Interface Sci.* **2004**, *9*, 213–221.

(8) Colloidal Biomolecules, Biomaterials, and Biomedical Aplications, In *Surfactant Science Series*; Elaïssari, A. Ed.; Marcel Dekker, Inc.: New York, 2003; *Vol. 126*.

(9) Gil, E. S.; Hudson, S. A. *Prog. Polym. Sci.* **2004**, *29*, 1173–1222.

(10) Rodriguez-Hernandez, J.; Checot, F.; Gnanou, Y.; Lecommandoux, S. *Prog. Polym. Sci.* **2005**, *30*, 691–724.

(11) Charles, M. H.; Charreyre, M. T.; Delair, T.; Elaissari, A.; Pichot, C. *Stp Pharma Sci.* **2001**, *11*, 251–263.

(12) *Nanomaterials for Medical Diagnosis and Therapy*, Kumar, C. S. S. R. Ed.; Wiley-VCH: Weinheim, 2007.

(13) Nayak, S.; Lyon, L. A. *Angew. Chem., Int. Ed.* **2005**, *44*, 7686–7708.

(14) Berndt, I.; Pedersen, J. S.; Richtering, W. *Angew. Chem., Int. Ed.* **2006**, *45*, 1737–1741.

(15) Schilli, C. M.; Zhang, M. F.; Rizzardo, E.; Thang, S. H.; Chong, Y. K.; Edwards, K.; Karlsson, G.; Muller, A. H. E. *Macromolecules* **2004**, *37*, 7861–7866.

(16) Kuckling, D.; Vo, C. D.; Wohlrab, S. E. *Langmuir* **2002**, *18*, 4263–4269.

(17) Suwa, K.; Yamamoto, K.; Akashi, M.; Takano, K.; Tanaka, N.; Kunugi, S. *Colloid Polym. Sci.* **1998**, *276*, 529–533.

(18) Seto, Y.; Aoki, T.; Kunugi, S. *Colloid Polym. Sci.* **2005**, *283*, 1137–1142.

(19) Pichot, C.; Taniguchi, T.; Delair, T.; Elaissari, A. *J. Disper. Sci. Technol.* **2003**, *24*, 423–437.

(20) Ballauff, M.; Lu, Y. *Polymer* **2007**, *48*, 1815–1823.

(21) Duracher, D.; Elaissari, A.; Mallet, F.; Pichot, C. *Langmuir* **2000**, *16*, 9002–9008.

(22) Silva, C. S. O.; Baptista, R. P.; Santos, A. M.; Martinho, J. M. G.; Cabral, J. M. S.; Taipa, M. A. *Biotechnol. Lett.* **2006**, *28*, 2019–2025.

(23) Elaissari, A.; Ganachaud, F.; Pichot, C. *Colloid Chem.* **2003**, *227*, 169–193.

(24) Elaïssari, A.; Ganachaud, F.; Pichot, C. *Top. Curr. Chem.* **2003**, *227*, 169.

(25) Prazeres, T. J. V.; Santos, A. M.; Martinho, J. M. G. *Langmuir* **2004**, *20*, 6834–6840.

(26) Prazeres, T. J. V.; Fedorov, A.; Martinho, J. M. G. *J. Phys. Chem. B* **2004**, *108*, 9032–9041.

(27) Pelton, R. *Adv. Colloid Interface Sci.* **2000**, *85*, 1–33.

(28) Jones, C. D.; Lyon, L. A. *Macromolecules* **2000**, *33*, 8301–8306.

(29) Berndt, I.; Pedersen, J. S.; Richtering, W. *J. Am. Chem. Soc.* **2005**, *127*, 9372–9373.

(30) Castanheira, E. M. S.; Martinho, J. M. G.; Duracher, D.; Charreyre, M. T.; Elaissari, A.; Pichot, C. *Langmuir* **1999**, *15*, 6712–6717.

(31) Santos, A. M.; Elaissari, A.; Martinho, J. M. G.; Pichot, C. *Polymer* **2005**, *46*, 1181–1188.

(32) Kubota, K.; Fujishige, S.; Ando, I. *J. Phys. Chem.* **1990**, *94*, 5154–5158.

(33) Fujishige, S.; Kubota, K.; Ando, I. *J. Phys. Chem.* **1989**, *93*, 3311–3313.

(34) Otake, K.; Inomata, H.; Konno, M.; Saito, S. *Macromolecules* **1990**, *23*, 283–289.

(35) Schild, H. G.; Tirrell, D. A. *J. Phys. Chem.* **1990**, *94*, 4352–4356.

(36) Pelton, R. H.; Pelton, H. M.; Morphesis, A.; Rowell, R. L. *Langmuir* **1989**, *5*, 816–818.

(37) Stockmayer, W. H. *Macrom. Chem. Phys.* **1960**, *35*, 54.

(38) Shibayama, M.; Tanaka, T. *Volume Phase Transition and Related Phenomena of Polymer Gels*; Springer-Verlag: Berlin, 1993; *Vol. 109*.

(39) Farinha, J. P. S.; Piçarra, S.; Miesel, K.; Martinho, J. M. G. *J. Phys. Chem. B* **2001**, *105*, 10536–10545.

(40) Piçarra, S.; Relogio, P.; Afonso, C. A. M.; Martinho, J. M. G.; Farinha, J. P. S. *Macromolecules* **2003**, *36*, 8119–8129.

(41) Ganachaud, F.; Elaissari, A.; Pichot, C.; Laayoun, A.; Cros, P. *Langmuir* **1997**, *13*, 701–707.

(42) Berndt, I.; Pedersen, J. S.; Lindner, P.; Richtering, W. *Langmuir* **2006**, *22*, 459–468.

(43) Farinha, J. P. S.; Charreyre, M. T.; Martinho, J. M. G.; Winnik, M. A.; Pichot, C. *Langmuir* **2001**, *17*, 2617–2623.

(44) Helfand, E.; Tagami, Y. *J. Chem. Phys.* **1972**, *56*, 3592–3601.

(45) Forster, T. *Ann. Phys. Leipzig.* **1948**, *2*, 55–75.

(46) Forster, T. *Z. Naturforsch. A* **1949**, *4*, 321–327.

(47) Farinha, J. P. S.; Martinho, J. M. G. *Resonance Energy Transfer in Polymer Interfaces, in Fluorescence of Supermolecules, Polymers and Nanosystems*; Berberan-Santos, M. N. Ed.; Springer-Verlag: Berlin, 2008.

(48) Fonseca, T.; Relogio, P.; Martinho, J. M. G.; Farinha, J. P. S. *Langmuir* **2007**, *23*, 5727–5734.

(49) Farinha, J. P. S.; Martinho, J. M. G. *J. Phys. Chem. C* **2008**, *112*, 10591–10601.

(50) Lakowicz, J. R. *Principles of Fluorescence Spectroscopy*; Kluwer Academic/Plenum: New York, 1999.

(51) Drake, J. M.; Klafter, J.; Levitz, P. *Science* **1991**, *251*, 1574–1579.

(52) Marcus, A. H.; Fayer, M. D. *J. Chem. Phys.* **1991**, *94*, 5622–5630.

(53) Marcus, A. H.; Diachun, N. A.; Fayer, M. D. *J. Phys. Chem.* **1992**, *96*, 8930–8937.

(54) Quitevis, E. L.; Marcus, A. H.; Fayer, M. D. *J. Phys. Chem.* **1993**, *97*, 5762–5769.

(55) Berberan-Santos, M. N.; Prieto, M. J. E. *J. Chem. Soc. Faraday Trans.* **1987**, *83*, 1391–1410.

(56) Schillen, K.; Yekta, A.; Ni, S. R.; Winnik, M. A. *Macromolecules* **1998**, *31*, 210–212.

(57) Farinha, J. P. S.; Schillen, K.; Winnik, M. A. *J. Phys. Chem. B* **1999**, *103*, 2487–2495.

(58) Duhamel, J.; Yekta, A.; Ni, S.; Khaykin, Y.; Winnik, M. A. *Macromolecules* **1993**, *26*, 6255–6260.

(59) Martin, T. J.; Webber, S. E. *Macromolecules* **1995**, *28*, 8845–8854.

(60) Johansson, L. B. A.; Blancharddesce, M.; Almgren, M.; Lehn, J. M. *J. Phys. Chem.* **1989**, *93*, 6751–6754.

(61) Kalman, B.; Clarke, N.; Johansson, L. B. A. *J. Phys. Chem.* **1989**, *93*, 4608–4615.

(62) Johansson, L. B. A.; Engstrom, S.; Lindberg, M. *J. Chem. Phys.* **1992**, *96*, 3844–3856.

(63) Yamazaki, I.; Tamai, N.; Yamazaki, T. *J. Phys. Chem.* **1990**, *94*, 516–525.

(64) Loura, L. M. S.; Fedorov, A.; Prieto, M. *Biophys. J.* **1996**, *71*, 1823–1836.
(65) Loura, L. M. S.; Fedorov, A.; Prieto, M. *J. Phys. Chem. B* **2000**, *104*, 6920–6931.
(66) Loura, L. M. S.; Fedorov, A.; Prieto, M. *Biophys. J.* **2001**, *80*, 776–788.
(67) Tamai, N.; Yamazaki, T.; Yamazaki, I. *Thin Solid Films* **1989**, *179*, 451–455.
(68) Tamai, N.; Yamazaki, T.; Yamazaki, I. *Can. J. Phys.* **1990**, *68*, 1013–1022.
(69) Farinha, J. P. S.; Martinho, J. M. G.; Kawaguchi, S.; Yekta, A.; Winnik, M. A. *J. Phys. Chem.* **1996**, *100*, 12552–12558.
(70) Pham, H. H.; Farinha, J. P. S.; Winnik, M. A. *Macromolecules* **2000**, *33*, 5850–5862.
(71) Farinha, J. P. S.; Vorobyova, O.; Winnik, M. A. *Macromolecules* **2000**, *33*, 5863–5873.
(72) Farinha, J. P. S.; Spiro, J. G.; Winnik, M. A. *J. Phys. Chem. B* **2001**, *105*, 4879–4888.
(73) Nakashima, K.; Duhamel, J.; Winnik, M. A. *J. Phys. Chem.* **1993**, *97*, 10702–10707.
(74) Nakashima, K.; Liu, Y. S.; Zhang, P.; Duhamel, J.; Feng, J. R.; Winnik, M. A. *Langmuir* **1993**, *9*, 2825–2831.
(75) Stryer, L.; Haugland, R. P. *Proc. Natl. Acad. Sci. USA* **1967**, *58*, 719–726.
(76) Haas, E.; Wilchek, M.; Katchalskikatzir, E.; Steinberg, I. Z. *Proc. Natl. Acad. Sci. USA* **1975**, *72*, 1807–1811.
(77) Deniz, A. A.; Laurence, T. A.; Beligere, G. S.; Dahan, M.; Martin, A. B.; Chemla, D. S.; Dawson, P. E.; Schultz, P. G.; Weiss, S. *Proc. Natl. Acad. Sci. USA* **2000**, *97*, 5179–5184.
(78) Lilley, D. M. J.; Wilson, T. J. *Curr. Opin. Chem. Biol.* **2000**, *4*, 507–517.
(79) Sekar, R. B.; Periasamy, A. *J. Cell Biol.* **2003**, *160*, 629–633.
(80) Zelazny, E.; Borst, J. W.; Muylaert, M.; Batoko, H.; Hemminga, M. A.; Chaumont, F. *Proc. Nat. Acad. Sci., USA* **2007**, *104*, 12359–12364.
(81) Meyer, P.; Dworkin, J. *Res. Microbiol.* **2007**, *158*, 187–194.
(82) Huebsch, N. D.; Mooney, D. J. *Biomaterials* **2007**, *28*, 2424–2437.
(83) Schillen, K.; Yekta, A.; Ni, S. R.; Farinha, J. P. S.; Winnik, M. A. *J. Phys. Chem. B* **1999**, *103*, 9090–9103.
(84) Dar, A. A.; Rather, G. M.; Das, A. R. *J. Phys. Chem. B* **2007**, *111*, 3122–3132.
(85) Junquera, E.; Aicart, E. *Langmuir* **2002**, *18*, 9250–9258.
(86) Spiro, J. G.; Farinha, J. P. S.; Winnik, M. A. *Macromolecules* **2003**, *36*, 7791–7802.
(87) Farinha, J. P. S.; Wu, J.; Winnik, M. A.; Farwaha, R.; Rademacher, J. *Macromolecules* **2005**, *38*, 4393–4402.
(88) Marquardt, D. W. *J. Soc. Ind. Appl. Math.* **1963**, *11*, 431–441.
(89) Farinha, J. P. S.; Martinho, J. M. G.; Pogliani, L. *J. Math. Chem.* **1997**, *21*, 131–139.
(90) Wang, X. H.; Qiu, X. P.; Wu, C. *Macromolecules* **1998**, *31*, 2972–2976.
(91) Brandrup, J.; Immergut, E. H. *Polymer Handbook*; Wiley: New York, 1989.
(92) Baumann, J.; Fayer, M. D. *J. Chem. Phys.* **1986**, *85*, 4087–4107.
(93) Yekta, A.; Winnik, M. A.; Farinha, J. P. S.; Martinho, J. M. G. *J. Phys. Chem. A* **1997**, *101*, 1787–1792.
(94) Farinha, J. P. S.; Martinho, J. M. G. *J. Lumin.* **1997**, *72*−*4*, 914–917.
(95) Murphy, M. C.; Rasnik, I.; Cheng, W.; Lohman, T. M.; Ha, T. J. *Biophys. J.* **2004**, *86*, 2530–2537.

JP804747B